IOP Publishing Smart Materials and Structures
Smart Mater. Struct. **23** (2014) 115007 (9pp) doi:10.1088/0964-1726/23/11/115007

Dynamically programmable surface micro-wrinkles on PDMS-SMA composite

Ping-Liang Ko[1], Fu-Long Chang[1], Chih-Hung Li[2], Jian-Zhang Chen[2], I-Chun Cheng[3], Yi-Chung Tung[4], Shih-Hang Chang[5] and Pei-Chun Lin[1]

[1] Department of Mechanical Engineering, National Taiwan University, No.1 Sec.4 Roosevelt Rd., Taipei 10617, Taiwan
[2] Graduate Institute of Applied Mechanics, National Taiwan University, Taipei 10617, Taiwan
[3] Department of Electrical Engineering & Graduate Institute of Photonics and Optoelectronics, National Taiwan University, Taipei 10617, Taiwan
[4] Research Center for Applied Sciences, Academia Sinica, Taipei 11529, Taiwan
[5] Department of Chemical and Materials Engineering, National I-Lan University, No.1 Sec.1 Shen-Lung Rd, I-Lan 26047, Taiwan

E-mail: jchen@ntu.edu.tw and peichunlin@ntu.edu.tw

Received 8 June 2014, revised 31 July 2014
Accepted for publication 28 August 2014
Published 25 September 2014

Abstract

We report on the development of a PDMS-SMA composite whose surface micro wrinkles can be dynamically programmed by an electrical current supplied to the SMA wire. It is advantageous over other techniques for surface topographical modulation, including portability, real-time programmability, no requirement for specific surface chemistry, operability under ambient conditions, and relative ease of control. A simplified mechanical model is also developed to describe the force-deflection balance of the PDMS-SMA composite. The wavelengths and amplitudes of the wrinkles when different currents applied to the SMA are characterized, and the experimental results agree with the theoretical model. The developed composite device can be applied to programmable modulations of surface adhesion, friction, wettability, etc.

Keywords: polydimethylsiloxane, composite, shape memory alloy, PDMS

(Some figures may appear in colour only in the online journal)

1. Introduction

Surface wrinkling is a form of instability occurring in mechanical systems [1–6]. Similar to buckling, surface wrinkling is also caused by a bifurcation in the solution of the equations of static equilibrium. When the strains of a thin hard layer and an adjacent soft bulk material are mismatched, the internal stress deforms the originally flat bi-layer structure into the sinusoidal waves on the surface [7, 8]. The transformation between flat and wrinkled is a surface geometrical change, and the dimensions of the wrinkles can be spread to several orders. Many applications have been developed using wrinkles within micro- and nano-scales—for example, control of cell alignment [9], generation of microlens arrays [10, 11], design of optical devices [12–16] (gratings) [17, 18], phase control of liquid crystals [19], design of semiconductors [20], tuning of surface adhesion [21], tuning of surface wettability [22–26], design of micro-fluidic devices [15, 26], control of shape of micro-droplets [27], and measurement of ultrathin films' properties [28–30].

These ordered surface wrinkles can be generated by several different methods: differential heat contraction [12, 17, 31], UV/ozone (UVO) treatment [10, 11, 24, 26, 31, 32], electrical inducement [16, 33, 34], surface pattern swelling [3, 5, 35], mechanical stretch or compression [2, 4, 6, 11, 13, 18–21, 25–28, 30, 36, 37], actuation of shape memory polymer [9], etc. However, these methods usually require sample fabrication or manipulation in well-controlled surroundings such as a temperature-controlled environment, UVO setting, electrical circuit layout, or solvent immersion; most of these are incompatible with the electricity-based control systems adopted in practical engineering

systems. In addition, the surface wrinkles generated by some methods lack a robust mechanism to be dynamically tuned in real time. All these constraints reduce the reliability and repeatability of surface wrinkle systems in daily engineering applications.

Previously, we reported on the fabrication and tuning of micro-scale surface wrinkles based on external mechanical force modulation. By simply stretching the polydimethylsiloxane (PDMS) sample and then performing oxygen plasma treatment, the self-organized wrinkles are permanently formed when the external stretching force is released [36]. Furthermore, depending on the strain releasing sequence of the two planar axes, pattern of the wrinkles can be generated in 1-dimensional (1D) wavy ripples, 2D random herringbone structure, or 2D zigzag highly-ordered herringbone structure. The external force modulation method is further utilized to fabricate a microlens array [11] and in-situ tuning of adhesion [21] and wettability [25]. Though the force method can easily be used in and translated to/from different ambient environments, having a human operator to apply the external forces in-situ is still inconvenient. If an automatic tuning system is desired, it is even more cumbersome to have a motorized system built next to the sample for the external force generation.

PDMS has been mixed with other materials to form smart functional composites [38–42]. These PDMS composites formed with PZT [38], carbon particles [42], and nickel particles/fibers [41] can be actuated via piezoelectric pressures, photothermal effects, and magnetic forces, respectively. Micro/nano-scale wrinkling patterns also have been realized on the surfaces of shape memory polymers (SMPs) via coatings of thin gold layers [43]. In comparison with shape memory alloys (SMAs), SMPs generally have a higher recoverable strain but a much lower recovery stress [43–46]; therefore, the actuation force of SMPs is usually lower. In this paper, aiming at automatic and programmable electrical-signal-based control on wrinkle formation and disappearance, we report on a composite made of PDMS and SMA. SMA allows large-scale thermal-induced deformation [47, 48], whereas PDMS elastomers can easily be oxidized with a thin silica layer on the surface to produce surface wrinkles using oxygen plasma treatment. By combining SMA and PDMS to form a composite, we are able to program or dynamically control the wrinkle formation and disappearance by widely-used electrical signals. Thus, a portable and controllable composite device for in-situ topologically changeable micro-wrinkles can be achieved; this device can further be used for tunings of wettability, adhesion, or friction.

The rest of the article is organized as follows. Section 2 describes the design concept, fabrication process, and modeling of the mechanism of the proposed PDMS-SMA composite. Section 3 presents the performance of the composite and discusses its behavior. Section 4 describes the experimental details, and section 5 concludes the work.

2. Design, fabrication, and modeling of the composite

2.1. Design concept and mechanism of the PDMS-SMA composite

Based on partially linear and partially nonlinear 1D stability analysis of a flat thin high-modulus layer attached to a semi-infinite low-modulus substrate [7, 8], if the compression strain (ε) of the thin layer passes the critical value (ε_c) [7, 8]

$$\varepsilon_c = \frac{1}{4}\left(\frac{3E_s\left(1-\nu_t^2\right)}{E_t\left(1-\nu_s^2\right)}\right)^{2/3}, \tag{1}$$

the thin layer exhibits buckling to form sinusoidal wrinkles. The notations E and ν are the Young's modulus and Poisson ratio, respectively, while the subscripts s and t accordingly indicate the substrate and thin layer. The wavelength of the wrinkles (λ) can be described as

$$\lambda = \frac{\pi t}{\sqrt{\varepsilon_c}}, \tag{2}$$

where t indicates the thickness of the thin layer. The amplitude of the wrinkle (A) can be given as [49, 50]

$$A = t\sqrt{\frac{\varepsilon}{\varepsilon_c} - 1}\,. \tag{3}$$

Note that amplitude is a function of (ε) but that wavelength is not. Thus, when the material is continuously compressed to a higher strain level, the wavelength theoretically stays at the same value but the amplitude increases accordingly. Our previous experimental investigation showed that the wavelength also decreased due to the effect of un-modeled high nonlinearity when the strain was sufficiently large [36].

Based on the phenomenon described above, if the thin hard layer is attached to the stretched elastic soft substrate with strain (ε_0) larger than the critical strain (ε_c), the elastic energy of the substrate compresses the thin hard layer and buckles it into a wrinkle form when the stretch is released. Theoretically the sample is at rest with a length at which the elastic force of the substrate balances the buckling force of the thin layer. Usually the substrate is much thicker than the thin layer (i.e., with large stiffness), so the sample can be restored close to its natural length (i.e., small strain of the substrate can create enough elastic force to balance the buckling force). In this case, the wrinkles of the sample can be stably formed without further assistance. When the sample is stretched to the level where the strain of the thin layer is less than the critical strain, the wrinkles of the thin layer disappear and revert to a flat state. As a result, the sample can dynamically change its state between flat and wrinkled with different amplitudes, depending on the strain applied to the sample.

The strain is a useful, convenient, and controllable factor for dynamic tuning of the sample surface, and its generation requires a force. Here, the Ni-Ti SMA wire is utilized as the force generator. If the SMA wire is embedded into the substrate with a length shorter than its 'memorized' length, and

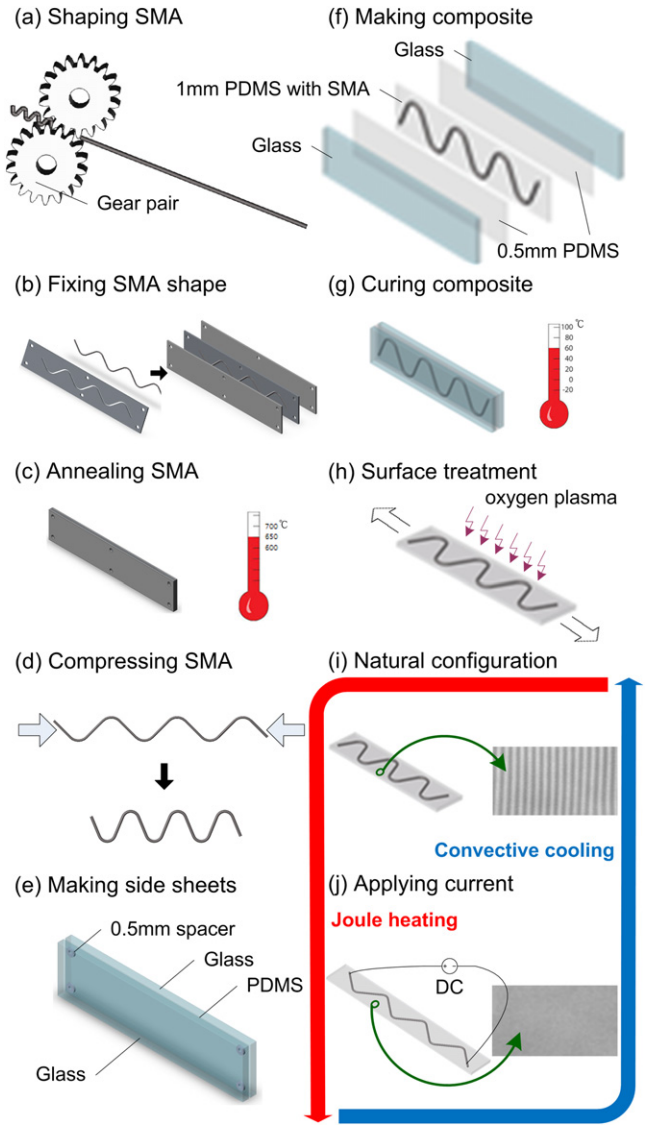

Figure 1. Illustration of the fabrication process of the PDMS-SMA composite with dynamically programmable surface micro-wrinkles.

the wire is passed with current (i.e., joule heating), the SMA tries to restore its original length, resulting in stretching of the substrate. The sample is balanced with the length where the elastic force from the substrate matches that from the SMA. In the meantime, the strain of the thin hard layer decreases, thus decreasing the amplitude of the wrinkle or further flattening the surface. As a result, by changing the current passing through the SMA, the wrinkle state can be tuned accordingly.

2.2. Fabrication process of the PDMS-SMA composite

The overall fabrication process and device operation procedure are depicted in figure 1. First of all, the SMA wire is deformed into a wavy shape by passing the SMA wires through a rolling gear pair as shown in figure 1(a). Second, the SMA wire is placed into a fixture which can confine the geometrical shape of the wire to prevent any possible deformation caused by the follow-up annealing process. The fixture is composed of two solid side plates and one middle plate with a wavy groove whose shape is identical to the SMA wires after rolling. As shown in figure 1(b), in this step, the wire is first placed within the groove and covered by two side plates, and then the three plates are screwed together. Next, the fixture with the wire is put into the oven for annealing as shown in figure 1(c). Owing to the shape memory nature of SMA, the deformation by cold working at below the transformation temperature may be recovered at higher temperature. Therefore, we constrain the SMA and anneal it at 650 °C for 1 h to define the SMA into a wavy shape. Next, the wire is taken from the fixture and compressed to a shorter length as shown in figure 1(d). The SMA is then embedded into the thin PDMS sheet as shown in figure 1(e). In this step two thin side PDMS sheets with a uniform thickness need to be made first. This can be achieved by molding the PDMS within two parallel glass sheets spaced at a fixed distance (i.e., thickness of the side sheet), and then removing one of the glass sheets after PDMS curing. The SMA wire is then sandwiched by these two PDMS side sheets with a fixed distance where the glass sheets are placed on the outer side. Then the uncured viscous PDMS liquid is filled into the gap (as shown in figure 1(f)) and cured (as shown in figure 1(g)). The curing process includes a room temperature stage and a follow-up elevated temperature curing. This strategy allows the PDMS to solidify to an elastomer, preventing the SMA from generating unwanted temperature-induced deformation when elevated temperature curing is applied. Next, the PDMS-SMA composite is stretched with a fixed strain by the external clamping jig and exposed to oxygen plasma, as shown in figure 1(h). After the process, a thin and rigid silica layer is generated on the PDMS surface. When the external stretched force is released, the PDMS-SMA composite is restored close to its natural length. In the meantime, the thin silica layer is simultaneously deformed into wrinkles as shown in figure 1(i). When an electric current is applied to the SMA wire, joule-heating increases the temperature of the wire which undergoes a phase transformation into parent phase. The SMA wire is elongated and balanced with a PDMS-bias spring. Thus, the PDMS-SMA will be stretched and the surface wrinkle will disappear as shown in figure 1(j). With this electrically-controlled deformation of the SMA, dynamic switching of the surface topography is achievable (i.e., switching between 1(i) and 1(j)). The photo of the fabricated composite is shown in figure 2(a).

2.3. The simplified motion model

The PDMS-SMA composite achieves the surface topography change by strain mismatch between the hard thin layer and the soft substrate, and the required forces for this deformation are from SMA (extension) and PDMS (restoration), respectively. The PDMS is one type of elastomers, and its force-deflection relation is reasonably approximated by an ordinary linear spring when the deformation is small. The force-deflection relation of the SMA is determined by two factors: memory effect and change of Young's modulus. When the SMA undergoes phase transformation at a certain temperature range, the two phases, Martensite (low temperature phase)

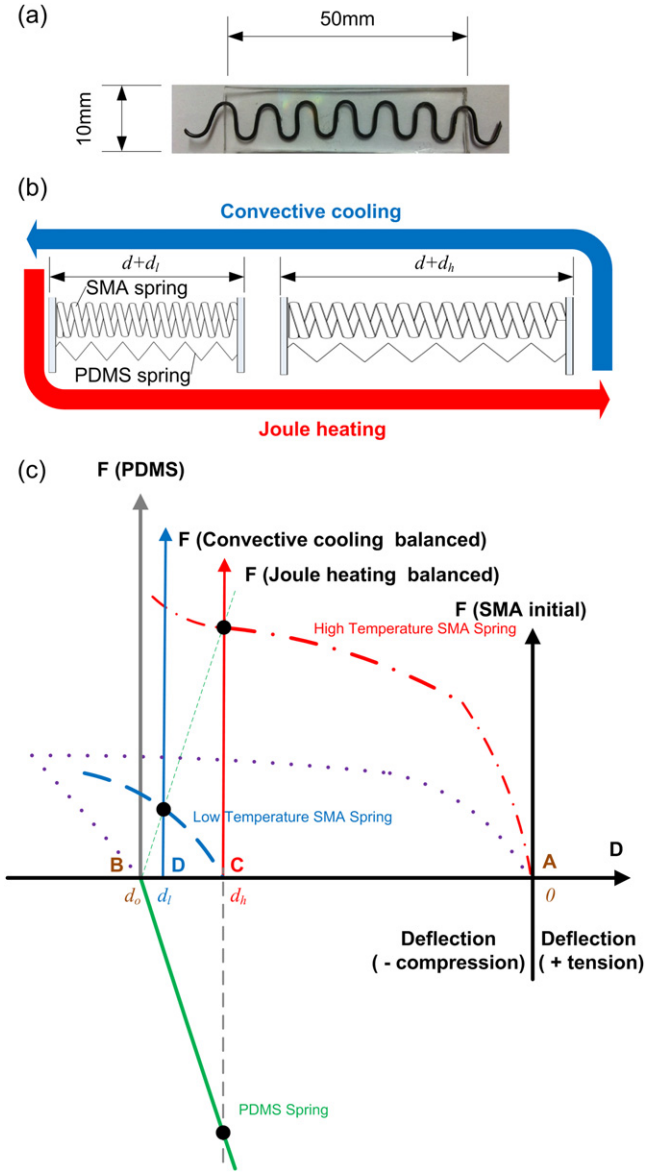

Figure 2. Force-deflection balancing model of the PDMS-SMA composite: (a) Photo of the composite; (b) Simplified two-spring model of the composite; (c) The force-deflection relation of the model.

and parent phase (high temperature), rest in different natural lengths as well as possess different Young's moduli. Besides PDMS and SMA, the generated hard thin layer on top of the PDMS also has a mechanical effect, but the resultant force of the layer is much smaller such that its force-deflection effect is ignored. As a result, the bi-directional sample deformation is dominated by the forces generated by the PDMS and the SMA, and this mechanism can be approximated as the parallel-connected SMA spring and PDMS spring as shown in figure 2(b). Because the memory effect of the SMA is one-way, the PDMS spring can be regarded as the 'bias spring' for the SMA, engaging SMA at a different length when the memory effect is not activated (i.e., no joule heating). This device is thus functioning as a two-way actuator [47]. As described in sub-section 2.2, the natural length of the PDMS spring is intentionally set to be shorter than the memorized-length of the SMA. As the temperature rises (i.e., device is joule heated), the composite is stretched to release the strain of the hard thin layer, flattening the wrinkles. On the other hand, when the temperature drops (i.e., convective cooling), the elastic force of the PDMS shortens the length of the sample, thus buckling the hard thin layer into wrinkles.

The length of the PDMS-SMA composite is balanced at the length where the forces generated in the PDMS and SMA are equal in magnitude but opposite in direction. Figure 2(c) depicts the force-deflection mechanism of the composite. Corresponding to figure 1(c), assuming the SMA is memorized with length d and has no externally applied force, it is operated at point A where is the origin of the SMA coordinate, as shown in figure 2(c). Next, corresponding to figure 1(d), it is largely compressed because deformation of the SMA passes the elastic range and reaches plastic regime. When the compression force releases, the SMA retains the deflection d_0 (i.e., minus sign). The operation point of the SMA is moved from point A to point B via the purple dotted curve as shown in figure 2(c). Note that the curve is the resultant 'force-deflection' relation of the wavy-shape SMA spring,' not the relation of the SMA itself. Referring to figure 1(g), because the PDMS is cured at this moment, its natural configuration is located at point B that is the origin of the PDMS coordinate. Its force-deflection relation is plotted as a solid green line. When the SMA is joule heated, the SMA tends to revert to its memorized length at point A because of the shape memory effect. However, owing to the existence of the PDMS spring, the final configuration of this composite is balanced with the deflection d_h (i.e., point C as shown in figure 2(c)); the forces generated in the PDMS and SMA are equal in magnitude but opposite in direction. Note that in this computation the force-deflection relation of SMA in high temperature condition should be used, which is plotted as a red dash-dotted curve, shown in figure 2(c). In short, the composite is stretched with length $d_h - d_0$ (i.e., positive sign) at high temperature by joule heating. When the sample temperature is lowered by convective cooling, one can assume that the new natural length as well as the force-deflection pattern of the SMA spring remains unchanged. In this case, the new origin of the SMA is located at point C, and the force-deflection relation of the SMA is depicted by the blue dashed curve, which has the same shape as the purple dotted curve but with its origin offset. Thus, when the composite cools down, it is balanced with deflection d_l, marked as point D in figure 2(c). The composite is compressed with length $d_l - d_h$ (positive sign). When the composite is heated again, the deflection goes back to point C. Afterward, the composite is balanced at point C upon heating and at point D upon cooling. Thus, the length change corresponding to the temperature change is $d_l - d_h$. Note that the PDMS and the SMA have thermal expansion as well, but the length change owing to this effect is small compared to the memory and spring effects, so thermal expansion is ignored in this model. It is worthwhile to note that the bulk PDMS is in fact interlocked with the SMA spring, so the force-deflection relations of the PDMS and SMA, as well as their interactions, is expected to

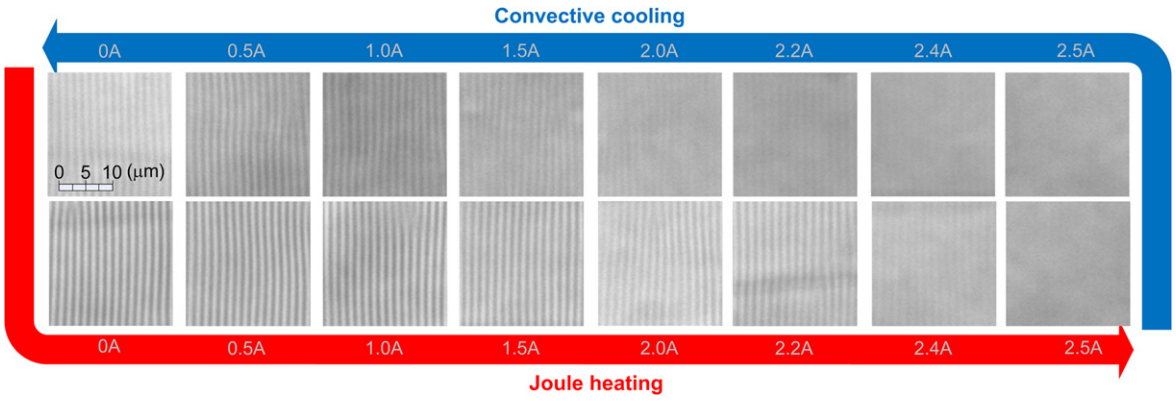

Figure 3. The sequential optical-microscope images of the PDMS-SMA composites when different currents are applied to the SMA wire.

be more complicated than the simplified parallel-spring model, which may result in a discrepancy between the experimental result and the prediction of this simplified model. Nevertheless, the simplified model provides insight into the deformation mechanism and a rough quantitative estimation of the composite.

3. Results and discussion

Figure 3 plots the micro-wrinkles observed by the optical microscope with different electric currents passed to the SMA wire embedded in the composite. When the current increases to 2.4 A, the clarity of the wrinkle pattern gradually decreases. When the current reaches 2.5 A, the hard thin layer is stretched back to a flat configuration and the pattern suddenly disappears. Note that the wavelength of the wrinkles remains roughly the same during the joule heating process. Owing to the light condensation by the wrinkles, the grey or white colors represent specific positions of the wave and the distance between two adjacent identical colors is equal to the wavelength of the wrinkles. The wavelength of the wrinkles is computed to be $\lambda = 1.479\,\mu$m by the Fast Fourier transform. On the other hand, during the heating process the clarity of the pattern gradually decreases, indicating the reduction of wrinkle amplitude and diminution of the light condensation. When the composite is cooled down, the wrinkles re-appear. The phenomenon of wrinkle formation and disappearance matches the phenomenon predicted by the model described in section 2.1.

The geometrical properties of the wrinkles are further characterized by the optical profiler as shown in figure 4, where 4(a) and 4(b) plot the peak-to-peak value (i.e., twice the amplitude of the wrinkle) and wavelength of the wrinkles versus current, respectively. When the current increases, the amplitude of the wrinkles decreases and their wavelength remains the same. Because of the thermal and hysteresis effects on the bulk PDMS, the wrinkle formation and disappearance happen at a slightly different current, but the trends generally match the optical microscope observations and the theoretical model. As the currents reach 2.4 and 2.2 A, the images shown on the optical profiler appear with visible

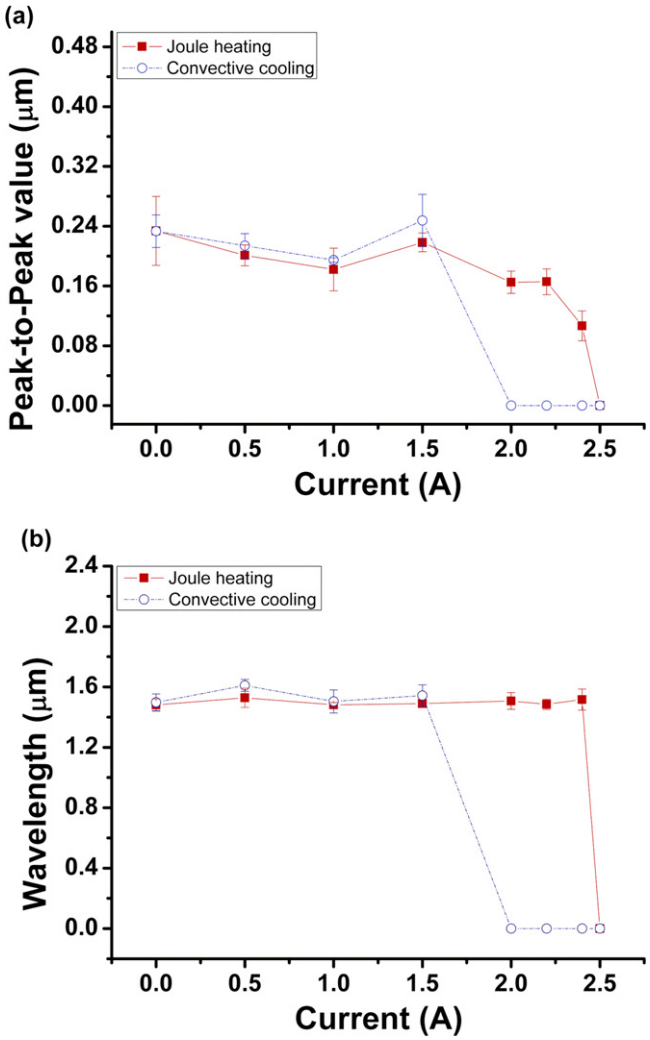

Figure 4. Amplitude peak-to-peak value (a) and wavelength (b) of the wrinkles on the surface of the PDMS-SMA composite.

wrinkles, the same as in the photos taken by the optical microscope. However, the automatic wave finder built with the instrument cannot identify the shallow wrinkles, so the software yields zero outputs of the wavelength and the amplitude. In summary, the measurement obtained from the optical profiler confirms that the design of this composite

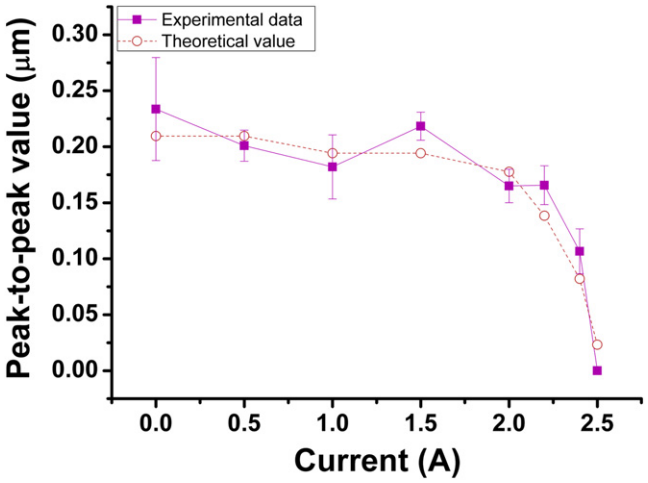

Figure 5. Comparison of peak-to-peak value of the wrinkles between theoretical and experimental results.

structure for wrinkle formation and disappearance is well-functioning.

Figure 5 plots the comparison of the amplitude peak-to-peak value versus current between the data measured from optical profiles and calculated from the theoretical model. The computation details are described as follows. The Young's modulus of the PDMS are experimentally measured to be $E_s = 1.4\ MPa$. The commonly-used Poisson ratio of the PDMS is $\nu_s = 0.5$, and Young's modulus and Poisson ratio of the oxidized hard thin layer are $E_t = 73.1\ GPa$ and $\nu_t = 0.17$. Together with measured wavelength $\lambda = 1.479\ \mu m$, by equation (1) the buckling strain is $\varepsilon_c = 4.42E - 4$. The thickness of the oxidized hard thin layer, t, is derived to be between 9.9 *nm* by equation (2), reasonably matching the values reported in other literature [2, 21, 51]. Next, together with the released strain $\varepsilon = 0.05$, the amplitude of the wrinkles can be yielded by equation (3). The amplitude of the wrinkles is $A_0 = 0.105\mu m$ when the composite is not heated. The amplitudes of the wrinkles at other current conditions can be computed in a similar manner, as plotted in figure 5. Note that, for plotting, the computed amplitudes are multiplied by two since the vertical axis of the figure indicates amplitude peak-to-peak value. The results shown in figure 5 reveal that the values of measured amplitudes agree with the theoretical calculations, which indicates that the mechanism for controlling the surface micro-wrinkles by the electricity is predictable as well as functional. This provides a valuable design guideline for future development when the surface topographical change is further utilized for other applications such as change of wettability and adhesion.

4. Experimental

4.1. PDMS-SMA composite fabrication

The Ni-Ti SMA wire and gear pair shown in figure 1(a) are commercially available. The diameter of the SMA (Nan-Cheng Co.) is 0.8 mm, and the S45C gear pair has 15 teeth and modulus of 4. The mold shown in figure 1(b) is made with steel and has thickness of 1 mm, and the groove is formed by laser cutting. The SMA wire is cut and inserted into the groove, at which the end-to-end length of the SMA spring is 160 *mm*. The annealing process shown in figure 1(c) is done in the oven (DF202, DENG YANG) at 650 °C for 1 h and cooled down to room temperature by air convection. In the process shown in figure 1(d), the apparent length of the SMA spring is compressed from 160 *mm* to 60 *mm* and then annealed. The PDMS is 184 Silicone Elastomer from Dow Corning® with mix ratio of 10:1. The thickness of the PDMS sheet shown in figure 1(e) is 0.5 *mm*, and is cured at 60 °C in the oven (Lindberg/Blue M™ LGO Box Furnaces, Thermo Scientific) for 12 h between two 10 *mm* thick glass plates. Two thin PDMS sheets are required. After removing one side glass plate of each PDMS-glass mold, the SMA wire is placed in the middle of these two thin PDMS sheets with a glass plate on the back. The spacing is controlled at 1 *mm*, and another batch of PDMS mixture is poured into the spacing to make the PDMS-SMA composite as shown in figure 1(f). The PDMS is first cured at room temperature for 12 h to prevent thermal-induced deformation of the SMA, and then cured at 60 °C in the oven for another 12 h to complete curing, as shown in figure 1(g). The thickness of the cured PDMS-SMA composite is 2 *mm*. The composite is cut into strips with a length of 50 *mm* and a width of 10 *mm*. The extra 5 *mm* of the SMA on each side is reserved for connecting to the power source for joule heating the SMA spring.

4.2. Wrinkle formation

The fabricated PDMS-SMA composite is stretched lenghtwise by 5% and fixed on the clamp to maintain its elongation. The stretched composite is then subjected to oxygen plasma treatment (PX-250, Nordson MARCH) for 10 min with power rating of 300 W as shown in figure 1(h). After the treatment, a thin and stiff oxidized siliceous layer is formed on the composite surface. After releasing the tension, the oxidized siliceous layer is buckled to form micro-wrinkles on the surface of the composite as shown in figure 1(i). After this initial formation, the stretch of the composite is actuated by elongation of the SMA via supplying current through the SMA wire. The commercial power supply (E3631A, Agilent) is used to provide the electrical power for SMA.

4.3. Wrinkle manipulation

The electrical power is the active control command to the composite. The formation and disappearance of the wrinkles is mainly determined by the length of the composite, which is further controlled by the thermal condition of the SMA. To understand the relation between the active control input and the thermal condition of the SMA, the quantitative relation among the voltage, current, and temperature of the SMA and PDMS-SMA composite was investigated, with the result shown in figure 6. The thermal distribution was taken by an infrared camera (TVS-500EX, NEC Avio Infrared Tech. Co.), and figure 6(a) shows an exemplary thermal image. Eight

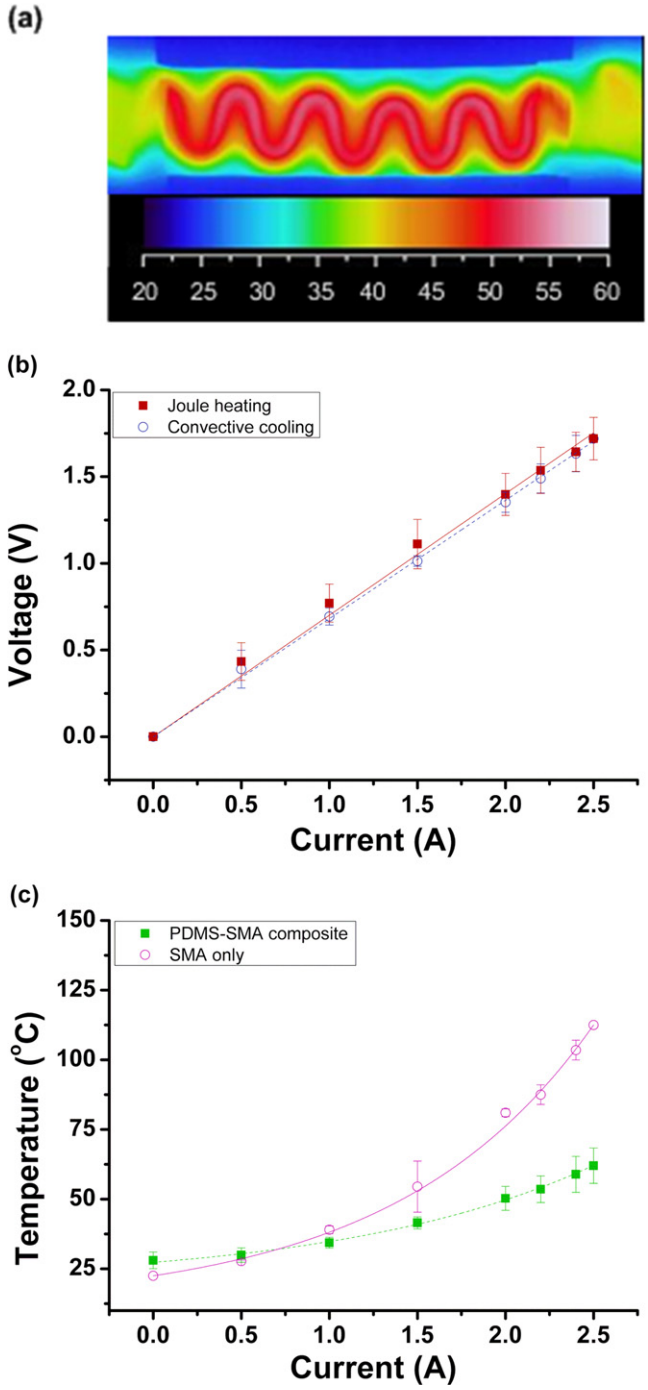

Figure 6. The thermal and electrical properties of the PDMS-SMA composite: (a) Thermal image of the PDMS-SMA composite; (b) Voltage vs. current of the SMA within the PDMS-SMA composite; (c) Temperature vs. currents of the bare SMA spring and PDMS-SMA composite.

different currents were sequentially supplied to the SMA: 0, 0.5, 1.0, 1.5, 2.0, 2.2, 2.4, and 2.5 A, each for 5 min, to reach thermal equilibrium. Figures 6(b) and (c) show the relations for voltage versus current and temperatures of the composite and bare SMA versus current, respectively. The voltage and current information is directly read from the power supply. The olive dashed line shows the surface temperature of the composite, and the pink solid line shows the temperature of only the SMA wire without the PDMS. The actual temperature of the SMA embedded within the PDMS-SMA composite lies in the region between these two temperature curves. The presented statistical result is the summary of several experimental runs. The monotonic variation confirms that the SMA temperature controlled by electricity is practical and repeatable.

4.4. Measurement

The images shown in figure 3 were taken by an optical microscope (DMI 6000 B, Leica). The wrinkles' profiles shown in figures 4 and 5 were taken by the optical profiler (VK-9710, KEYENCE). The Young's moduli of the PDMS and the SMA spring were experimentally measured. Both were measured by the same setup, and here the setup for PDMS is described as the demonstration. The PDMS strip was placed vertically and clamped on both sides. One end was connected to a heavy weight and mounted on the electronic scale with a resolution of 0.5 g, and the other end was hung from the top with a screw system, which can stretch PDMS precisely by small amounts. After the PDMS was carefully clamped on the system with natural length, the scale was reset to zero. Next, the PDMS was gradually stretched by designated amounts while the readings on the scales were recorded. The stretch was then gradually released by the same method. The stretch-release process was repeated several times without interruption, so that the force-deflection relation of the initial movement and the follow-up movement (i.e., with plastic deformation) could be recorded. The force-deflection of the SMA spring at room temperature was obtained by the same method. That of the SMA spring at parent phase (high temperature phase) was found in a similar manner, except that the SMA wire was soaked in the beaker with hot water.

5. Conclusions

We report on the design of a PDMS-SMA composite with dynamically programmable surface micro-wrinkles. Simply by applying oxygen plasma treatment on the stretched PDMS elastomer, an oxidized siliceous hard thin layer forms on top of the PDMS surface. When the stretch force is released, the elastic force of the PDMS returns the PDMS back to its natural configuration, and the micro-scale wrinkles automatically generate owing to the mechanical instability induced by the strain mismatch between the hard thin layer and the elastic bulk PDMS material. More importantly, the surface topography can be in-situ and repeatedly varied between high wrinkles and flat surfaces, depending merely on the stretch level of the sample. To make the surface-topography-changeable system portable and programmable, Ni-Ti SMA wire with a memorized length longer than the natural configuration of the PDMS is embedded within the PDMS through a multi-step fabrication process. Thus, when the electrical current is applied to the SMA wire, the joule heat changes the phase of the SMA between Martensite and parent

phases, resulting in the change of Young's modulus and the recovery force which stretches the PDMS-SMA and flattens the composite surface. When no current is applied, the elastic force of the PDMS shortens the composite and forms the wrinkle. Therefore, based on this internal and bi-directional force balance mechanism, the surface wrinkles can be dynamically programmed simply by electrical signals. A simplified mechanical model was also developed to describe the force-deflection balance of the PDMS-SMA composite, which takes the Young's modulus change and natural configuration change into account. The wavelengths and amplitudes of the wrinkles while different currents are applied to the SMA are characterized. When the current gradually increases, the wavelength of the wrinkles observed by the optical microscope and optical profiler remains at roughly the same value, and the amplitude of the wrinkles decreases. When the current reaches 2.5 A, the wrinkles disappear. The quantitative topographical behavior of the wrinkles matches that estimated by the theoretical model. The compact design and simple programmability of the proposed PDMS-SMA composite can be readily deployed into various empirical applications, such as programmable surface adhesion, friction, wettability, etc.

Acknowledgments

The authors gratefully acknowledge the support from the Ministry of Science and Technology of Taiwan with grant numbers NSC 102-2221-E-002-060 and MOST 103-2221-E-002-057, as well as from the National Taiwan University with grant number NTU-CDP-102R7817. The authors also wish to express their gratitude toward Prof. Wen-Pin Shih, Department of Mechanical Engineering at National Taiwan University, for access to the thermography equipment.

References

[1] Yoo P J and Lee H H 2008 Complex pattern formation by adhesion-controlled anisotropic wrinkling *Langmuir* **24** 6897–902
[2] Yang S, Khare K and Lin P-C 2010 Harnessing surface wrinkle patterns in soft matter *Advanced Functional Materials* **20** 2550–64
[3] Tanaka T, Sun S-T, Hirokawa Y, Katayama S, Kucera J, Hirose Y and Amiya T 1987 Mechanical instability of gels at the phase transition *Nature* **325** 796–8
[4] Jiang C, Singamaneni S, Merrick E and Tsukruk V V 2006 Complex buckling instability patterns of nanomembranes with encapsulated gold nanoparticle arrays *Nano Lett.* **6** 2254–9
[5] Klein Y, Efrati E and Sharon E 2007 Shaping of elastic sheets by prescription of non-euclidean metrics *Science* **315** 1116–20
[6] Zhang Y, Matsumoto E A, Peter A, Lin P-C, Kamien R D and Yang S 2008 One-step nanoscale assembly of complex structures via harnessing of an elastic instability *Nano Lett.* **8** 1192–6
[7] Allen H G 1969 *Analysis and Design of Structural Sandwich Panels* (London: Pergamon)
[8] Genzer J and Groenewold J 2006 Soft matter with hard skin: From skin wrinkles to templating and material characterization *Soft Matter* **2** 310–23
[9] Yang P, Baker R M, Henderson J H and Mather P T 2013 *In vitro* wrinkle formation via shape memory dynamically aligns adherent cells *Soft Matter* **9** 4705–14
[10] Chan E P and Crosby A J 2006 Fabricating microlens arrays by surface wrinkling *Adv. Mater.* **18** 3238–42
[11] Chandra D, Yang S and Lin P-C 2007 Strain responsive concave and convex microlens arrays *Appl. Phys. Lett.* **91** 251912–3
[12] Koo W H, Jeong S M, Araoka F, Ishikawa K, Nishimura S, Toyooka T and Takezoe H 2010 Light extraction from organic light-emitting diodes enhanced by spontaneously formed buckles *Nat. Photonics* **4** 222–6
[13] Lee S G, Lee D Y, Lim H S, Lee D H, Lee S and Cho K 2010 Switchable transparency and wetting of elastomeric smart windows *Adv. Mater.* **22** 5013–7
[14] Yoo P 2011 Invited paper: Fabrication of complexly patterned wavy structures using self-organized anisotropic wrinkling *Electronic Materials Letters* **7** 17–23
[15] Kim H S and Crosby A J 2011 Solvent-responsive surface via wrinkling instability *Adv. Mater.* **23** 4188–92
[16] van den Ende D, Kamminga J-D, Boersma A, Andritsch T and Steeneken P G 2013 Voltage-controlled surface wrinkling of elastomeric coatings *Adv. Mater.* **25** 3438–42
[17] Bowden N, Brittain S, Evans A G, Hutchinson J W and Whitesides G M 1998 Spontaneous formation of ordered structures in thin films of metals supported on an elastomeric polymer *Nature* **393** 146–9
[18] Harrison C, Stafford C M, Zhang W and Karim A 2004 Sinusoidal phase grating created by a tunably buckled surface *Appl. Phys. Lett.* **85** 4016–8
[19] Ohzono T and Monobe H 2012 Microwrinkles: Shape-tunability and applications *J. Colloid Interface Sci.* **368** 1–8
[20] Khang D-Y, Jiang H, Huang Y and Rogers J A 2006 A stretchable form of single-crystal silicon for high-performance electronics on rubber substrates *Science* **311** 208–12
[21] Lin P-C, Vajpayee S, Jagota A, Hui C-Y and Yang S 2008 Mechanically tunable dry adhesive from wrinkled elastomers *Soft Matter* **4** 1830–5
[22] Peng Y T, Lo K F and Juang Y J 2010 Constructing a superhydrophobic surface on polydimethylsiloxane via spin coating and vapor-liquid sol-gel process *Langmuir* **26** 5167–71
[23] Rahmawan Y, Moon M W, Kim K S, Lee K R and Suh K Y 2010 Wrinkled, dual-scale structures of diamond-like carbon (DLC) for superhydrophobicity *Langmuir* **26** 484–91
[24] Chung J Y, Youngblood J P and Stafford C M 2007 Anisotropic wetting on tunable micro-wrinkled surfaces *Soft Matter* **3** 1163–9
[25] Lin P-C and Yang S 2009 Mechanically switchable wetting on wrinkled elastomers with dual-scale roughness *Soft Matter* **5** 1011–8
[26] Khare K, Zhou J and Yang S 2009 Tunable open-channel microfluidics on soft poly(dimethylsiloxane) (PDMS) substrates with sinusoidal grooves *Langmuir* **25** 12794–9
[27] Xia D, Johnson L M and López G P 2012 Anisotropic wetting surfaces with one-dimesional and directional structures: fabrication approaches, wetting properties and potential applications *Adv. Mater.* **24** 1287–302
[28] Stafford C M, Harrison C, Beers K L, Karim A, Amis E J, VanLandingham M R, Kim H-C, Volksen W, Miller R D and Simonyi E E 2004 A buckling-based metrology for measuring the elastic moduli of polymeric thin films *Natural Materials* **3** 545–50
[29] Huang J, Juszkiewicz M, de Jeu W H, Cerda E, Emrick T, Menon N and Russell T P 2007 Capillary wrinkling of floating thin polymer films *Science* **317** 650–3

[30] Chung J Y, Chastek T Q, Fasolka M J, Ro H W and Stafford C M 2009 Quantifying residual stress in nanoscale thin polymer films via surface wrinkling *ACS Nano* **3** 844–52
[31] Bowden N, Huck W T S, Paul K E and Whitesides G M 1999 The controlled formation of ordered, sinusoidal structures by plasma oxidation of an elastomeric polymer *Appl. Phys. Lett.* **75** 2557–9
[32] Chung J Y, Nolte A J and Stafford C M 2009 Diffusion-controlled, self-organized growth of symmetric wrinkling patterns *Adv. Mater.* **21** 1358–62
[33] Schaffer E, Thurn-Albrecht T, Russell T P and Steiner U 2000 Electrically induced structure formation and pattern transfer *Nature* **403** 874–7
[34] Lin Z, Kerle T, Baker S M, Hoagland D A, Schaffer E, Steiner U and Russell T P 2001 Electric field induced instabilities at liquid/liquid interfaces *The Journal of Chemical Physics* **114** 2377–81
[35] Chan E P and Crosby A J 2006 Spontaneous formation of stable aligned wrinkling patterns *Soft Matter* **2** 324–8
[36] Lin P-C and Yang S 2007 Spontaneous formation of one-dimensional ripples in transit to highly ordered two-dimensional herringbone structures through sequential and unequal biaxial mechanical stretching *Appl. Phys. Lett.* **90** 241903
[37] Yang Y, Han X, Ding W L, Jiang S C, Cao Y P and Lu C H 2013 Controlled free edge effects in surface wrinkling via combination of external straining and selective O-2 plasma exposure *Langmuir* **29** 7170–7
[38] Babu I, Hendrix M M R M and de With G 2014 PZT-5A4/PA and PZT-5A4/PDMS piezoelectric composite bimorphs *Smart Materials and Structures* **23** 025029
[39] Wu R, Han M W, Lee G Y and Ahn S H 2013 Woven type smart soft composite beam with in-plane shape retention *Smart Materials and Structures* **22** 125007
[40] Li W H and Nakano M 2013 Fabrication and characterization of PDMS based magnetorheological elastomers *Smart Mater. Struct.* **22** 055035
[41] Zhu L, Xie D S, Ma J, Shao J and Shen X Q 2013 Fabrication of polydimethylsiloxane composites with nickel particles and nickel fibers and study of their magnetic properties *Smart Mater. Struct.* **22** 045015
[42] Pimentel-Dominguez R, Sanchez-Arevalo F M, Hautefeuille M and Hernandez-Cordero J 2013 Laser induced deformation in polydimethylsiloxane membranes with embedded carbon nanopowder *Smart Mater. Struct.* **22** 037001
[43] Zhao Y, Huang W M and Fu Y Q 2011 Formation of micro/nano-scale wrinkling patterns atop shape memory polymers *J. Micromech. Microeng.* **21** 067007
[44] Yang B, Huang W M, Li C and Li L 2006 Effects of moisture on the thermomechanical properties of a polyurethane shape memory polymer *Polymer* **47** 1348–56
[45] Tobushi H, Hara H, Yamada E and Hayashi S 1996 Thermomechanical properties in a thin film of shape memory polymer of polyurethane series *Smart Materials and Structures* **5** 483–91
[46] Huang W 2002 On the selection of shape memory alloys for actuators *Materials Design* **23** 11–9
[47] Kyung-Tae L, Gil-Yong L, Jung-Oh C, Renzhe W and Sung-Hoon A 2010 Design and fabrication of a smart flexible structure using shape memory alloy wire (SMA) *2010 3rd IEEE RAS and EMBS Int. Conf. on Biomedical Robotics and Biomechatronics (BioRob)* pp 599–603
[48] Liang C and Rogers C A 1992 Design of shape memory alloy actuators *Journal of Mechanical Design* **114** 223–30
[49] Chen X and Hutchinson J W 2004 Herringbone buckling patterns of compressed thin films on compliant substrates *ASME Journal of Applied Mechanics* **71** 597–603
[50] Huang Z Y, Hong W and Suo Z 2005 Nonlinear analyses of wrinkles in a film bonded to a compliant substrate *J. Mech. Phys. Solids* **53** 2101–18
[51] Hellmich W, Regtmeier J, Duong T T, Ros R, Anselmetti D and Ros A 2005 Poly(oxyethylene) based surface coatings for poly(dimethylsiloxane) microchannels *Langmuir* **21** 7551–7